

MILITARY TECHNICAL COLLEGE
CAIRO - EGYPT7th INTERNATIONAL CONF. ON
AEROSPACE SCIENCES &
AVIATION TECHNOLOGY**PENETRATION OF A LONG ROD INTO A SEMI-INFINITE
METALLIC TARGET AT HIGH VELOCITY**

by

A. M. Riad *

ABSTRACT

The one-dimensional hydrodynamic theory proposed by Tate [1,2] is considered as a standard reference for describing the penetration of long rods into semi-infinite metallic targets. In this paper, a modified analytical approach using Tate's theory has been developed, wherein the penetration process is considered to consist of three phases: hydrodynamic, deformation and rigid. These phases are related to the situations of the rod front during target penetration. For each rod phase, the target penetration is described consisting of two stages: erosion and deformation. The plastic wave theory is used with the equations of motion to predict the sequence of penetration stages that associate with each rod penetration phase and represent the complete penetration process. In addition, the strength factors for both rod and target materials, respectively, are assumed not to vary during their erosion.

The governing equations of the analytical approach are programmed using FORTRAN. The input data consist of rod impact velocity, length, diameter, density and Brinell hardness number as well as target density, Young's modulus and Brinell hardness number. The present results are concerned with the predictions of the produced hole diameter and penetration depth in semi-infinite targets due to their impact by long rods with high velocities. The predicted results are compared with the experimental results of other investigators; good agreement is obtained. Moreover, the program is used to discuss the influence of the different penetration parameters on penetration depth and produced hole diameter.

KEY WORDS

- Dynamics
- Solid Mechanics
- Impact Dynamics
- Penetration Mechanics
- Impact of Solids

* Dept. Mech. Engng., M. T. C., Cairo, Egypt.

INTRODUCTION

Higher impact velocities, i.e. greater than 1000 m/s, tend to generate erosion of both rod and target materials, respectively. The modified hydrodynamic theories of penetration, introduced by Tate [1,2] and Alekseevskii [3], have been widely used as simple models for describing the penetration of long rods into semi-infinite metallic targets. These models predict both the penetration depth and the deceleration of the rod. Both models contain two strength factors, R_t and Y_p for target and rod materials, respectively. These factors are determined experimentally. Tate [1] used the Hugoniot elastic limit (HEL) of the rod material for Y_p and a value of $3.5 \times (\text{HEL})$ of the target material for R_t .

Hohler and Stilp [4] investigated the penetration mechanism of steel and high density rods into semi-infinite steel targets of different yield strengths using an impact velocity range between 500 and 4000 m/s. Their experimental results prove that the depth of rod penetration is increased due to the increase of the rod density, yield strength and impact velocity. For a constant length to diameter ratio of the rod, the crater volume is increased with impact velocity. In addition, their experimental program shows that the values of the strength factors, R_t and Y_p , agree with Tate's suggestion.

Tate [5,6] developed a flow field model to describe the transient, plastic-wave dominated and after flow phases of hydrodynamic penetration. Through this model, he derived the relationships between both rod and target strength factors and their dynamic yield strengths. He also derived a formula for estimating the crater diameter. The results of his model are concerned with the predictions of the rod penetration depth through the target and the diameter of the produced hole.

Jones et al. [7] modified Tate's work (cf. Ref. [1]) to incorporate the mushroom-type deformation at the impact end of the rod and the deceleration of the rigid end. The predicted penetration depths using Tate's theory are inconsistent with those predicted by Jones et al. modified theory for the same material strength factors. They attributed this difference to the lack of mushroom at the penetration tip in Tate's theory. Wilson et al. [8] carried out an experimental program to confirm the validity of the theory of Jones et al. Comparison between experimental results and Jones et al. predictions gave a quite good agreement. Wilson et al. recommended that a very good agreement could be obtained between predicted and experimental results if a velocity-dependent mushroom strain were considered in the model.

Another approach to the hydrodynamic theory of a long rod penetration into a semi-infinite target has been developed by Rosenberg et al. [9]. Their analysis was based on equating the forces on both sides of the moving rod-target interface assuming that the effective cross-sectional area of the mushroomed end of the rod was at least twice the value of its rigid part. For the target strength factor, they adopted an analytical expression resulting from the cylindrical cavity expansion theory. This factor, R_t , was found equal to a value of 3-4 times the compressive yield strength of the target material. Good agreement is obtained between the predicted results of their model and the experimental results over a narrow range of impact velocity.

In the following, an analytical approach describing the penetration process of a rod into a semi-infinite metallic target has been developed. The model identifies three rod phases: hydrodynamic, deformation and rigid. For each rod phase, the model defines two stages for target penetration: erosion and deformation; the one-dimensional impulse-momentum equation

is used to derive the main equations representing each stage of target penetration. The developed model is completely analytical; no empirical parameters are needed to run the model.

The governing equations of the model are compiled into a FORTRAN program. The input data to the program are easily determined. The model is capable of predicting the time-histories of the velocities of rod moving parts, penetration depth, rod non-deformed length and diameter of the produced hole. The present results of the developed model are concerned with the predictions of the final value of the rod penetration depth and the diameter of the produced hole at the target surface. The predicted results are compared with the experimental results of other investigators; good agreement is obtained. Moreover, the model is used to discuss the influence of the different penetration parameters on the rod penetration depths and produced hole diameters.

GOVERNING EQUATIONS OF THE DEVELOPED MODEL

In the following, the developed model identifies three phases for rod penetration into target; these phases are named: hydrodynamic, deformation and rigid. These phases accompany the rod front during its penetration through the target. For each rod phase, the target penetration stages are named: erosion and deformation. The one-dimensional impulse momentum equation is used to derive the main equations representing each target penetration stage.

Hydrodynamic Penetration Phase

In this phase, the rod impacts the semi-infinite target with velocity V_i higher than the hydrodynamic transient velocity V_{HT} . The transient velocity is defined as the impact velocity at which the rod front just starts to erode. Due to the high-speed impact, plastic wave cannot leave the interface and shock wave is generated and stands at the rod-target interface [10]. The pressure behind the shock wave is very high; any rod or target material passing through this interface has been eroded.

(i) Target erosion stage

The penetrator is a cylindrical rod; it has an initial length L_0 , density ρ_p and diameter D_0 . Let V_i denote the initial velocity of rod with which it impacts the semi-infinite target. After time t has elapsed, the rod has penetrated the target to a depth Z (cf. Fig. 1a). In the process, a portion of the rod of length X has been consumed. The remaining portion of the rod has a length $L_0 - X$ and a mass M_1 ; it is assumed to move as a rigid body with current velocity V . The rod penetrates the target with velocity U . If the cross-sectional area of the rod is denoted by A_0 , the force retarding the rigid body is approximately $A_0 Y_p$; where Y_p is defined as the pressure at which the rod material behaves like a fluid or the strength factor of the rod material.

Figure 1a also shows the rigid end of the rod at time $t + \Delta t$. A portion of the rod end has been consumed by the penetration process and the remaining rod end has been decelerated. It is simple to apply the one-dimensional impulse-momentum equation. Because of the forces F_1 ($= A_0 Y_p$) are equal and opposite, only the external force P contributes to the impulse. As it is opposite to the directions of U and V , its contribution is negative: $-P\Delta t$. The total momentum at time t is $\rho_p A_0 (L_0 - X)V$ and at time $t + \Delta t$ is $[\rho_p A_0 \Delta X(U + \Delta U) + \rho_p A_0 (L_0 - X - \Delta X)(V + \Delta V)]$. Subtracting to obtain the momentum change and equating this to impulse gives:

$$-P \Delta t = \rho_p A_o [(L_o - X) \Delta V - \Delta X (V - U) - \Delta X (\Delta V - \Delta U)], \quad (1)$$

Dividing through by Δt and taking the limits as Δt approaches zero gives:

$$-P = \rho_p A_o [(L_o - X) \frac{dV}{dt} - \frac{dX}{dt} (V - U)]. \quad (2)$$

From the definition $l = L_o - X$, Eqn. (2) can be rewritten as:

$$-P = \rho_p A_o [l \frac{dV}{dt} + \frac{dl}{dt} (V - U)]. \quad (3)$$

To get the internal force F_1 , as function of the rod non-deformed length l , the rod velocity V and the penetration velocity U , take the momentum of the element which is consumed at time t and time $t + \Delta t$. The momentum at time t is $\rho_p A_o \Delta X V$ and at time $t + \Delta t$ is $\rho_p A_o \Delta X (U + \Delta U)$. Subtracting to obtain the momentum change, equating the momentum change to impulse, dividing through by Δt and taking the limits as Δt approaches zero gives:

$$F_1 - P = -\rho_p A_o \frac{dl}{dt} (U - V). \quad (4)$$

From the Eqns. (3) and (4), the force F_1 is represented by:

$$F_1 - P = -A_o Y_p = A_o \frac{d}{dt} (\rho_p l V) + \rho_p A_o V (V - U). \quad (5)$$

During the time interval Δt , the back end of the remaining rod moves a distance $V\Delta t$ whilst its front moves $U\Delta t$. The change of length Δl is $(U - V)\Delta t$ so that:

$$\frac{dl}{dt} = - (V - U). \quad (6)$$

Substituting Eqn. (6) into Eqn. (5), the equation of motion of the rod rigid part is represented by:

$$Y_p = -\rho_p l \frac{dV}{dt}. \quad (7)$$

The rate of change of the depth of penetration, Z , with respect to time, t , is given by:

$$\frac{dZ}{dt} = U. \quad (8)$$

The modified Bernoulli equation which equates the pressure on both sides of the moving rod-target interface is represented by [1]:

$$\frac{1}{2} \rho_t U^2 + R_t = \frac{1}{2} \rho_p (V-U)^2 + Y_p, \quad (9)$$

where ρ_t is the density of the target material and R_t is the strength factor of the target material. Using Eqn. (9), the current penetration velocity, U , during the hydrodynamic penetration phase as a function of the current velocity of the rod rigid part, V , is represented by:

$$U(V) = \frac{1}{1-\mu^2} [V - \mu \sqrt{V^2 + A}], \quad (10)$$

where

$$\mu = \sqrt{(\rho_t / \rho_p)}, \quad (10a)$$

and

$$A = \frac{2(R_t - Y_p)(1 - \mu^2)}{\rho_t}. \quad (10b)$$

The following relations are used to determine analytically the strength factors of rod and target materials, respectively [6]:

$$Y_p = 1.7 \sigma_{yp}^D, \quad (11)$$

and

$$R_t = \sigma_{yt}^D \left(\frac{2}{3} + \ln \left(0.57 * \frac{E_t}{\sigma_{yt}^D} \right) \right), \quad (12)$$

where σ_{yt}^D and σ_{yp}^D are the dynamic yield strengths of rod and target materials, respectively, and E_t is Young's modulus of the target material. The dynamic yield strength is determined using Reicht principle [10] as follows:

$$\sigma_y^D \text{ [MPa]} = 3.92 \times HB, \quad (13)$$

where HB is the Brinell hardness of the material.

The current diameter of the produced cavity, D_c , at each incremental time Δt is determined using the following equation [6]:

$$\left(\frac{D_c}{D_o} \right)^2 = \left[1 + \left(\frac{2 \rho_p (V-U)^2}{R_t} \right) \right]. \quad (14)$$

Equations (6), (7) and (8) are a system of first order dependent differential equations; this system is solved numerically. The initial conditions are:

$$\text{at } t = 0, V = V_i, l = L_o, Z = 0.$$

Equation (10) is used to determine the penetration velocity U at each incremental time Δt . The solution gives the velocity of the rod rigid part V , the length of the rod rigid part l and the rod penetration depth Z as functions of the penetration time t . In addition, the diameter of the produced hole D_c can be obtained as a function of penetration time t using Eqn. (14).

There are three conditions to terminate the current stage: (i) $V-U = C_p$ and $U > C_t$, (ii) $V-U > C_p$ and $U < C_t$, and (iii) $l = 0$. For condition (i), the velocity of the rod rigid part V is equal to the transient velocity V_{HT} . At this velocity, the shock wave at the rod front is diminished and plastic wave starts to propagate from the interface through the rod material. Thus the target erosion stage of the rod deformation phase follows the current stage. Moreover, the length of the rod rigid part l at the end of this stage is considered as the initial length for the subsequent stage. The diameter of the rod front is considered to equal the diameter of the cavity at the end of this stage. In addition, the plastic wave travelling time through the rod material will be equal to $(t-t_p)$; where t_p is the penetration time until the current stage is terminated. For condition (ii), the target deformation stage of the rod hydrodynamic phase follows the current stage. For condition (iii), the rod is totally consumed and no further penetration will occur. In this case the whole penetration process is terminated.

To determine the transient velocity V_{HT} , substitute into Eqn. (9) for $(V-U) = C_p$. The value of the transient velocity depends on the relation between the strength factors of both rod and target materials. If $R_t > Y_p$, the transient velocity is determined using the following relation [6]:

$$V_{HT} = C_p + \left(\frac{C_p^2 - V_c^2}{\mu^2} \right)^{\frac{1}{2}} \quad (15)$$

Equation (15) determines the transient velocity for the case of $C_p > V_c$. Tate [6] considered that the hydrodynamic transient velocity was equal to V_c when the plastic wave velocity through the rod material is less or equal to the value V_c . The term V_c which has a velocity dimension is defined by:

$$V_c = (2 [R_t - Y_p] / \rho_p)^{\frac{1}{2}} \quad (16)$$

If $R_t < Y_p$, the transient velocity is determined using the following equation [6]:

$$V_{HT} = C_p + (V_t^2 + \left(\frac{C_p}{\mu} \right)^2)^{\frac{1}{2}} \quad (17)$$

where the term V_t which has a velocity dimension is represented by:

$$V_t = ([2 (Y_p - R_t)] / \rho_t)^{\frac{1}{2}} \quad (18)$$

If $R_t = Y_p$, the transient velocity is determined by:

$$V_{HT} = C_p \left(1 + \frac{1}{\mu}\right) \quad (19)$$

The plastic wave velocity through the rod material, C_p , is determined using the following equation [6]:

$$C_p = \left(\frac{1.86 B}{\rho_p}\right)^{\frac{1}{2}}, \quad (20)$$

where

$$B \text{ [MPa]} = 4.55 \times (HB)_p \quad (20) a$$

B is the work hardening coefficient of the rod material, and $(HB)_p$ is its Brinell hardness number.

(ii) Target deformation stage

This stage takes place when the velocity of the rod rigid part V is greater than the transient velocity V_{HT} and the penetration velocity U is less than the plastic wave velocity through the target material C_t . During this stage, the target material which is in contact with the rod front is plastically deformed whereas the rod front is still eroded (cf. Fig. 1a). At time t , the rod rigid mass is denoted by M_1 and the target deformed mass is denoted by M_3 . During target penetration, the mass of the rod rigid part decreases while the mass of the target deformed part increases. The shear stress that acts on the periphery of the target deformed part is neglected. Moreover, the diameter of the interface area is assumed to be equal to the diameter of the hole when the target erosion stage is terminated.

The main equations representing the current stage are:

- (a) the rate of change of the length of rod rigid part l with respect to penetration time t , Eqn. (6),
- (b) the equation of motion of rod rigid part, Eqn. (7),
- (c) the rate of change of rod penetration depth Z with respect to penetration time t , Eqn. (8), and (d) the equation of motion of target deformed part which is represented by:

$$\rho_t A_c C_t (t - t_1) \frac{dU}{dt} = Y_p A_o + \rho_p A_o (V - U)^2 - \sigma_t A_c - \rho_t A_c C_t U, \quad (21)$$

where t_1 is the time at which the erosion of the target surface is terminated, A_c is the interface area due to the contact of the rod front with target, $C_t (= [1.86 B_t / \rho_t]^{1/2}$; where B_t is the work hardening coefficient of target material) is the plastic wave velocity through the target material and σ_t is the constrained dynamic yield stress of the target material which acts on plastic wave front [11].

Equations (6), (7), (8) and (21) are a system of first order dependent differential equations; this system is solved numerically. The initial conditions to solve this system are:

$$\text{at } t = t_1, \quad V = V_{te}, \quad U = U_{te}, \quad l = l_{te}, \quad Z = Z_{te}, \quad D_c = D_{c_{te}}$$

where the subscript "te" means target erosion. So, the initial parameters for the current stage

are the end parameters of the target erosion stage. The solution gives the velocity of the rod rigid part V , the length of the rod rigid part l , the rod penetration depth Z and the penetration velocity U as functions of the penetration time t .

There are two conditions to terminate the current stage: (i) $V = V_{HT}$ and $U < C_p$, and (ii) $V > 0$ and $U = 0$. For condition (i), the target deformation stage of the rod deformation phase follows the current stage. The end conditions of the present stage are the initial conditions for the subsequent stage. For condition (ii), no further penetration of the rod through the target takes place. If the remaining rod rigid part has a velocity V , the remaining rod is considered to impact into a rigid surface. By applying Taylor theory [12], the final length of the remaining rod is determined using the following equation:

$$l_f = l_c \exp \left[-\frac{\rho_p V^2}{2 Y_p} \right], \quad (22)$$

where l_f is the final length of the remaining rod, l_c is the length of the remaining rod when the penetration velocity U is equal to zero and C_p is the plastic wave velocity through the rod material.

Rod Deformation Phase

In this phase, the plastic wave propagates from the interface through the rod material. The plastic wave divides the rod material into two parts: (i) rigid part, which has a mass M_1 and moves with velocity V , and (ii) deformed part, which has a mass M_2 and moves with the penetration velocity U (cf. Fig. 1b). The stress that acts at the plastic wave front is the dynamic yield strength of the rod material, σ_p [11]. The rod presented area on target is denoted by $A_c (= \pi/4 D_c^2)$ and is assumed to equal the rod presented area when the hydrodynamic phase is terminated. The principle of mass conservation is used to determine the height of the rod deformed part H at each incremental time Δt under the assumption that the rod front has a frustum shape.

For target material that is in contact with the rod front, two penetration stages could be associated with the present phase (cf. Fig. 1b). These stages are named: (i) target erosion, and (ii) target deformation. For target erosion stage, the penetration velocity U is greater than the plastic wave velocity through the target material C_t . The target strength factor R_t should be reduced due to the increase in rod penetration depth and the decrease in rod velocity. In this stage, the target strength factor is assumed not to vary during target erosion.

For target deformation stage, The plastic wave propagates from the interface through the target material. The target mass M_3 between the interface and the plastic wave front moves with the penetration velocity U . The pressure acting at the wave front is equivalent to the constrained dynamic yield strength of the target material and is denoted by σ_t . Moreover, the shear stress that acts on the periphery of target deformed part is neglected.

(i) Target erosion stage

The main equations of the current stage are derived assuming that it follows the target erosion stage of the hydrodynamic penetration phase. By applying the impulse-momentum equation in one dimension and mass conservation principle, the main equations representing the current stage are:

- (a) the rate of change of penetration depth Z with respect to penetration time, Eqn. (8),
- (b) the equation of motion of rod rigid part which is represented by:

$$\rho_p (l_{HT} - C_p(t-t_p)) \frac{dV}{dt} = -\sigma_p, \quad (23)$$

(c) the rate of change of length of rod rigid part with respect to time which is represented by:

$$\frac{dl}{dt} = -C_p, \quad (24)$$

and (d) the equation of motion of the rod deformed part which is:

$$\rho_p A_o C_p (t-t_p) \frac{dU}{dt} = \sigma_p + \rho_p A_o C_p (V-U) - R_t A_c - \rho_t A_c U^2, \quad (25)$$

Equations (8), (23), (24) and (25) are a system of first order dependent differential equations; this system is solved numerically. The initial conditions to solve this system are:

$$\text{at } t = t_p, \quad V = V_{HT}, \quad U = U_{HT}, \quad l = l_{HT}, \quad Z = Z_{HT},$$

where the subscript "HT" means hydrodynamic transient. So, the initial parameters for the current stage are equivalent to the parameter values when the velocity of rod rigid part V is equal to the transient velocity V_{HT} . The solution gives the velocity of the rod rigid part V, the length of the rod rigid part l, the rod penetration depth Z and the penetration velocity U as functions of the penetration time t. The length of rod deformed part H can be also determined as a function of the penetration time t.

There are two conditions to terminate the current stage: (i) $V=U$ and $U > C_t$, and (ii) $V-U < C_p$ and $U < C_t$. For condition (i), the rod penetrates the target as a rigid body while the target surface in contact with the rod is still eroded; the target erosion stage of the rod rigid phase follows the current stage. For condition (ii), both the rod front and the target material in contact with the rod front are deformed; the target deformation stage of the rod deformation phase follows the current stage. The end conditions of the present stage are the initial conditions for the subsequent stage.

(ii) Target deformation stage

The main equations representing the current stage are:

- (a) the rate of change of the rod penetration depth Z with respect to time, Eqn. (8),
- (b) equation of motion of rod rigid part, Eqn. (23),
- (c) the rate of change of the length of rod rigid part with respect to time, Eqn. (24), and
- (d) the equation of motion of rod and target deformed parts which is:

$$\rho_p A_o C_p (t-t_p) + \rho_t A_c C_t (t-t_1) \frac{dU}{dt} = A_o (\sigma_p + \rho_p C_p (V-U)) - A_c (\sigma_t + \rho_t C_t U). \quad (26)$$

The previous equations represent a system of first order dependent differential equations. The initial conditions to solve this system are dependent on the end conditions of the stage which precedes the present stage. The solution gives the velocity of the rod rigid part V, the length

of the rod rigid part l, the rod penetration depth Z and the penetration velocity U as functions of the penetration time t. The length of rod deformed part H can be also determined as a function of the penetration time t.

There are two conditions to terminate the current stage: (i) $U = V$ and $U < C_1$, and (ii) $V > 0$ and $U = 0$. For condition (i), the rod rigid phase terminates the penetration process; the target deformation stage of the rod rigid phase follows the current stage. For condition (ii), no further penetration of the rod through the target takes place. Moreover, the remaining rod rigid part is deformed assuming that it impacts into a rigid surface. Equation (22) is used to determine the final length of the remaining rod.

Rod Rigid Phase

The present phase follows the rod deformation phase in which the target erosion (i.e. $U > C_1$) or target deformation (i.e. $U < C_1$) takes place (cf. Fig. 1c). In this phase, the plastic wave propagation through the rod material is diminished. In addition, the rod completes the penetration process as a rigid body $M (=M_1+M_2)$. The one-dimensional impulse-momentum equation is applied to derive the main equations representing the following penetration stages:

(i) Target erosion stage

The main equations of the present stage are:

- (a) the rate of change of rod penetration depth with respect to time, Eqn. (8), and
- (b) the equation of motion of the rod which is represented by:

$$M \frac{dU}{dt} = -\rho_c A_c U^2 - R_c A_c \tag{27}$$

where M is the rod mass at the end of rod deformation phase. Equations (8) and (27) are solved numerically; the initial conditions to solve these equations are the end conditions of the target erosion stage which is associated with the rod deformation phase. The solution gives the rod penetration velocity U and the rod penetration depth Z as functions of penetration time t.

There are two conditions to terminate the current stage: (i) $0 < U < C_1$ and (ii) $U = 0$. For condition (i), the target erosion is terminated and deformation of target material which is in contact with rod front takes place. For condition (ii), the rod stops to penetrate the target and penetration process is terminated.

(ii) Target deformation stage

The main equations of the current stage are:

- (a) the rate of change of rod penetration depth with respect to time, Eqn. (8), and
- (b) the equation of motion of the rod and target deformed parts which is represented by:

$$[M + \rho_c A_c (t - t_1)] \frac{dU}{dt} = -\rho_c A_c U^2 - \sigma_c A_c \tag{28}$$

Equations (8) and (28) are a system of first order dependent differential equations. This system is solved numerically. The initial conditions to solve these equations are the end conditions of the target erosion stage which is associated with the rod rigid phase or the end

conditions of the target deformation stage which is associated with the rod deformation phase. The solution gives the rod penetration velocity U and the rod penetration depth Z as functions of time t . This stage is terminated when the penetration velocity U vanishes and the penetration process is completed.

The complete penetration process consists of a combination of the different stages which associate with the different rod phases. The sequences of the penetration stages are determined according to the relation between the relative velocity between the rod parts, $V - U$, and the plastic wave velocity through the rod material as well as the relation between the penetration velocity through the target and the plastic wave velocity through the target material.

RESULTS AND DISCUSSIONS

The present model is capable of predicting the time-histories of velocities of rod parts, lengths of rod parts and rod penetration depth which associate with the penetration of semi-infinite target by long rods. In the following, the present results are concerned with the predictions of the rod penetration depths and the diameters of the produced holes in semi-infinite targets due to their impact by long rods at high velocities. The model predictions are compared with the experimental results of other investigators. Moreover, the model is used to study the influence of the different penetration parameters on penetration depths and diameters of the produced holes.

(i) Validation of the Predicted Results of the Developed Model

The predicted results of the developed model is validated with the experimental measurements of depths of penetration obtained by Tate [1]. He studied the penetration of a high-speed soft steel rod into a semi-infinite soft steel target. Both the soft steel rod and target materials have the same dynamic yield strength of 650 MPa. The rod has a length of 63.5 mm and a length to diameter ratio of 10. The predicted depths of penetration and the corresponding experimental values obtained by Tate are listed in Table 1. Good agreement is found between the predictions of the present model and the corresponding experimental values.

The predicted results of the present model are also compared with the experimental and predicted results obtained by Hohler and Stilp [4]. They studied the penetration of a high-speed D17 tungsten rod into D17 tungsten and Hzb20 semi-infinite steel targets. The tungsten rod has a dynamic yield strength of 1060 MPa, a length of 62.5 mm and a diameter of 6 mm. The tungsten target has the same dynamic yield strength as the tungsten rod whereas the steel target has a dynamic yield strength of 1160 MPa.

The predicted depths of penetration due to the impact of tungsten rods into tungsten and steel targets, respectively, versus rod impact velocity are depicted into Figs. 2a and 3a. In addition, Figs. 2b and 3b depict the predicted surface hole diameters into tungsten and steel targets, respectively, versus rod impact velocity. The predicted results and experimental measurements of depths of penetration and surface hole diameters obtained by Hohler and Stilp are depicted on their respective figures. The comparison between the predicted model results and the results obtained by Hohler and Stilp shows good predictive capability of the developed model.

Another validation of the present model is performed herein. The predictive capability of the present model is tested using the same data for both rod and target materials that are examined by Kinsey and Zukas [13]. They tested the penetration of a high-speed C110W2 steel rod into a semi-infinite Hzb20 steel target. The target has a dynamic yield strength of

Table 1. Comparison between the predicted depths of penetration and the corresponding experimental measurements obtained by Tate [1].

Ser. No.	Impact velocity V_i [m/s]	Experimental penetration depth [1] [mm]	Predicted penetration depth, Z [mm]
1	1219	12.7	12.4
2	1890	38.1	40.1
3	1950	40.1	41.7
4	2347	43.2	50.2

850 MPa. The rod has a dynamic yield strength of 1050 MPa, a length of 43 mm and a length to diameter ratio of 10. Their theoretical results were predicted using a Lagrangian numeric code, EPIC-II.

Figure 4a plots the predicted change of the depths of penetration with rod impact velocity. The predicted depths of penetrations and the experimental values obtained by Kimsey and Zukas are depicted on the same figure. Moreover, Fig. 4b plots the predicted hole diameters using the present model as well as the predicted hole diameters and the corresponding experimental values obtained by Kimsey and Zukas. It is clear from both figures that the predicted depths of penetration and hole diameters using the present model are in good agreement with the results obtained by Kimsey and Zukas.

(ii) Effect of Penetration Parameters on Penetration Process

In the following, the present model is used to study the effect of the different penetration parameters on penetration process. The penetration parameters are classified into: (i) rod parameters, and (ii) target parameters. Rod parameters include rod length, diameter, yield strength and density, whereas the target parameters include target yield strength and density.

The present model investigates the effect of each parameter on the penetration of a high-speed rod into a semi-infinite metallic target individually. For each parameter, the depths of penetration and the surface hole diameters are predicted and are used to elaborate its effect on penetration process. In addition, the effect of each parameter on penetration process is supported with the available results of other investigators. Table 2 lists the input data of rod and target that are fed into the program to predict the effect of each parameter on penetration process. The theoretical results of the present model are predicted due to the interaction of rod and target having the same or different materials.

(a) Rod parameters

Effect of rod length

To study the effect of rod length on penetration process, the program is run considering three different lengths for the D17 tungsten rods. The considered rods are assumed to impact semi-infinite H_zB₂₀ steel targets with different velocities. The input data for rod and target that are fed into the program are listed in Table 2. The predicted change of depth of penetration with rod impact velocity for the different rod lengths is shown in Fig. 5.

Table 2. Input data to the computer program to study the effect of each penetration parameter on penetration process.

Parameter	Rod data						Target data				Remark Rod versus Target
	L ₀ [mm]	D ₀ [mm]	HB	Mat. Code	ρ _p [g/cm ³]	σ _{yp} ^D [MPa]	ρ _t [g/cm ³]	HB	σ _{yt} ^D [MPa]	Mat. Code	
Rod length	30 62.5 90	6	270	D17	17	1060	7.85	296	1160	HxB20	Tungsten versus Steel
Rod diameter	62.5	3 6 9	270	D17	17	1060	17	270	1060	D17	Tungs. versus Tungs.
Rod yield strength	62.5	6	96 216 296	1020 - Hz B20	7.85	375 850 1160	7.85	195	765	RHA	Steel versus Steel
Rod density	62.5	6	270	D17	17	1060	7.85	195	765	RHA	Tungsten versus Steel Steel versus Steel
Target yield strength	62.5	6	270	D17	17	1060	7.85	95 195 296	375 765 1160	1020 RHA 4340	Tungsten versus Steel
Target density	62.5	6	296	Hz B20	7.85	1160	2.75 7.85	166	650	- -	Steel versus Aluminium Steel versus Steel

It is clear from the figure that the predicted depths of penetration increase with increasing both rod length and impact velocity. During penetration, the rod front is consumed and/or deformed whereas the rear part of the rod moves as a rigid body with high velocity. For the same impact velocity, the length of remainder rigid part of the rod increases with rod length; this part acts on the base of the produced cavity during penetration. The kinetic energy of the rod remainder that dissipates into target penetration is directly proportional to the rod remainder length (mass). So, the depth of penetration increases with rod length. For the same rod length, the penetration velocity of rod through the target increases due to the increase of rod impact velocity. The depth of rod penetration is dependent on the penetration velocity. So, the depth of penetration increases with increasing the impact velocity.

Moreover, the program predicts the hole diameter through the target. For the considered rod lengths, the predicted hole diameters have the same value at the same impact velocity. So, the produced hole diameter into target is insensitive to the rod length. This could be attributed to the fact that the present model describes the rod penetration into a semi-infinite target in one-dimension. This prediction is also consistent with that obtained by Tate who models the hydrodynamic penetration in one dimension [1].

To defeat the modern armours, the ammunition designers look for the parameters which increase the penetration capability of the kinetic energy projectiles. It was found by experiments that the increase in length to diameter ratio increases the depth of penetration of a rod into a semi-infinite target [4]. Nowadays, the modern kinetic energy projectile is constructed to have a high length to diameter ratio; this ratio exceeds a limit of 20 (e.g. 115 mm armour piercing fin stabilized discarded sabot).

Effect of rod diameter

The program is run considering three different diameters for the D17 tungsten rods. These rods impact into semi-infinite D17 tungsten targets with different velocities. The input data to the program for both rod and target are listed in Table 2. Figure 6 plots the predicted change of hole diameter with rod impact velocity for the different rod diameters. It is evident from the figure that the diameters of the produced holes increase due to the increase of both rod impact velocity and rod diameter. This is attributed to the energy transferred from the rod to flow and displace the target material in-contact with the rod front. This energy increases with increasing the rod impact velocity and rod diameter (mass).

Effect of rod dynamic yield strength

The model is used to analyze the impact of steel rods having three different values of dynamic yield strength into semi-infinite rolled homogenous armours. The input data to the program for studying the effect of dynamic yield strength of rod material on penetration process are listed in Table 2. The predicted change of depth of penetration with rod impact velocity for the different values of dynamic yield strength of rod materials is depicted in Fig. 7a; whereas Fig. 7b depicts the predicted change of hole diameter with rod impact velocity for the same dynamic yield strengths of the considered rods.

For the same impact velocity, it is clear from Fig. 7a that the depth of penetration slightly increases with the increase in the dynamic yield strength of rod material. This is attributed to the small increase in penetration velocity due to the increase in dynamic yield strength of rod material. The predicted results of the present model indicate that the effect of yield strength of rod materials on the high-speed penetration of the semi-infinite targets could be neglected. This is due to the change of the rod front from the solid state to the fluid state. However, the depth of penetration increases with impact velocity for the same yield strength of rod; this is due to the increase in penetration velocity with impact velocity.

For the same impact velocity, Fig. 7b shows the increase in predicted hole diameter due to the decrease in dynamic yield strength of rod material. This is attributed to the excess deformation that the rod front of low dynamic yield strength suffers at impact. The increase in rod presented area (area of rod front) on target for the soft rod produces a hole of large diameter. In addition, the produced hole diameter increase with rod impact velocity for the same dynamic yield strength of rod; this is due to the increase in rod projected area on target with impact velocity.

Effect of rod density

Two different values of rod densities are considered to predict the effect of rod density on the depth of penetration of rod in target and hole diameter vacated by rod. Tungsten and steel rods are considered to impact into semi-infinite rolled homogenous armours. The input data that characterize rod and target are listed in Table 2; these data are fed into the program. Figures 8a and 8b plot the predicted changes of depth of penetration and hole diameter with rod impact velocity for different rod densities.

It is evident from both figures that the predicted penetration depth and hole diameter increase by increasing the rod density. These results are also verified experimentally by Hohler and Stulp [4]. They attributed this effect to the existence of a residual velocity for the remaining material of the dense rod in impact direction. This residual velocity prevents the rod material to stop on crater wall and pushes it towards the penetration direction. Therefore, a secondary penetration is obtained in addition to the primary penetration. Finally, the total depth of penetration for the dense rod increases.

The effect of rod density on the predicted depth of penetration could be also attributed to the dynamic pressure that acts on target material during penetration process. It is known that the dynamic pressure is function of rod density and rod velocity. For the same impact velocity, the applied pressure on target by a tungsten rod is higher than that applied by a steel one. Therefore, the depth of penetration increases when the dense rod penetrates the target. Similarly, the dynamic pressure acts on the wall of the vacated hole by rod; the hole diameter also increases by increasing the rod density (cf. Fig. 8b).

It was found by experiments that the projectile density is an important parameter for increasing the penetration capability of the kinetic energy projectiles. Nowadays, the modern kinetic energy projectiles are made from high dense materials such as tungsten alloys and depleted uranium.

(ii) Target parameters

Effect of dynamic yield strength of target

To study the effect of target dynamic yield strength on penetration process, the program is run considering three different values of dynamic yield strength of semi-infinite steel targets. Tungsten rods are considered to impact into steel targets with different velocities. The input data to the program for rod and target are listed in Table 2. Figure 9a depicts the predicted change of depth of penetration with rod impact velocity for the different values of target dynamic yield strengths; whereas Fig. 9b depicts the predicted change of hole diameter with rod impact velocities for the same values of target dynamic yield strengths.

For the same impact velocity, It is clear from Fig. 9a that the predicted depth of penetration decreases due to the increase of dynamic yield strength of target material. This is attributed to the small resistance of target material of low dynamic yield strength against rod penetration. The dynamic pressure applied on the bottom of the cavity pushes the target

material of low strength and penetrates it more deeply. Moreover, the depth of penetration increases with impact velocity for the same dynamic yield strength; this is due to the increase of dynamic pressure that acts on target material with impact velocity.

Christman and Gehring [14] studied experimentally the penetration of a high-speed rod into a semi-infinite target. They derived an empirical equation based on their experimental measurements for the determination of the depth of rod penetration into target. This equation shows that the depth of penetration is indirectly proportional to target hardness. Therefore, the depth of penetration decreases with increasing the dynamic yield strength of target.

For the same impact velocity, Fig. 9b shows that the predicted hole diameter is indirectly proportional to the dynamic yield strength of target material. This is attributed to the small resistance and excessive plastic flow of target material of low strength due to rod penetration. For the same yield strength, Fig. 9b also shows that the hole diameter increases with impact velocity. The increase in hole diameter is affected by the dynamic pressure that acts on the bottom of the cavity as well as the wall of cavity. For target material of low yield strength, the pressure pushes the wall and produces a hole of large diameter.

Effect of target density

Two different values of target densities are considered to predict their effect on penetration process. Target materials are considered to be aluminium and steel. Steel rods are considered to impact the abovementioned targets with different velocities. The input data to the program that characterize rod and target are listed in Table 2. The predicted changes of depth of penetration and hole diameter with rod impact velocity for different target densities are plotted on Figs. 10a and 10b.

For the same impact velocity, it is evident from Fig 10a that the predicted depth of penetration has a largest value when the target has low density. This is because the high penetration velocity of rod through a low density target. The empirical equation derived by Christman and Gehring [14] shows that the depth of penetration is indirectly proportional to target density. Moreover, Fig. 10b shows that the hole diameter increases with target density. This could be attributed to the pressure that acts on bottom and wall of the cavity and the time taken while the pressure is applied on target material. For dense target, the rod penetrates the target with small penetration velocity. Due to the small depth of penetration, the pressure acts on the wall of the cavity for long time and produces a hole of larger diameter.

CONCLUSIONS

An analytical model has been developed to describe the penetration of high-speed long rods into semi-infinite metallic targets. The model identifies three different phases for rod: hydrodynamic, deformation and rigid. For each rod phase, the model describes two stage for target penetration named: erosion and deformation. The governing equations for each perforation stage are derived and programmed using FORTRAN. The input data to run the program are easily determined.

The present results of the developed model are concerned with the predictions of depths of penetration and hole diameters. A comparison between the model predictions with the experimental measurements of other investigators is done; good agreement is obtained. In addition, the present model is used to study the effect of individual penetration parameters on penetration process. It is ascertained that the rod density and length to diameter ratio are the

major parameters for increasing the depth of rod penetration into target. Nowadays, these parameters are considered during the design and manufacturing of modern kinetic energy projectiles to increase their penetration capabilities. In addition, the increase in yield strength of rod has a very small effect on the increase in depth of penetration due to the change of rod front from solid to liquid state when the penetration process by high-speed rods starts. The present results indicate the predictive capabilities of the developed model.

REFERENCES

1. Tate, A., 'A Theory for the Deceleration of Long Rods after Impact', *J. Mech. Phys. Solids*, Vol. 15, pp. 387-399 (1967).
2. Tate, A., 'Further Results in the Theory of Long Rod Penetration', *J. Mech. Phys. Solids*, Vol. 17, pp. 141-150 (1969).
3. Alekseevskii, V.P., 'Penetration of a rod into a Target at High Velocity', *Combustion, Explosion and Shock Waves*, No. 2, pp. 63-66 (1966).
4. Hohler, V., and Stilp, A.J., 'Penetration of Steel and High Density Rods In Semi-Infinite Steel Targets', *Proc. 3 rd Int. Symp. Ballistics, Karlsruhe* (1977).
5. Tate, A., 'Long Rod Penetration Models-Part I. A Flow Field Model for High Speed Long Rod Penetration', *Int. J. Mech. Sci.*, Vol. 28, pp. 535-548 (1986).
6. Tate, A., 'Long Rod Penetration Models-Part II. Extensions to the Hydrodynamic Theory of Penetration', *Int. J. Mech. Sci.*, Vol. 28, pp. 599-612 (1986).
7. Jones, S.E., Gillis, P.P., and Foster, J.C., 'On the Penetration of Semi-Infinite Targets by Long Rods', *J. Mech. Phys. Solids*, Vol. 35, pp. 121-131 (1987).
8. Wilson, L.L., Foster, J.C., Jr, Jones, S.E. and Gillis, P.P., 'Experimental Rod Impact Results', *Int. J. Impact Engng.*, Vol. 8, pp. 15-25 (1989).
9. Resonberg, Z., Marmor, E., and Mayseless, M., 'On the Hydrodynamic Theory of Long-Rod Penetration', *Int. J. Impact Engng.*, Vol. 10, pp. 483-486 (1990).
10. Recht, R.F., 'Taylor Ballistic Impact Modelling Applied to Deformation and Mass Loss Determination', *Int. J. Engng. Sci.*, Vol. 16, pp. 809-827 (1978).
11. Yuan, W., Lanting, Z., Xiaoging, M., and Strong, W., 'Plate Perforation by Deformable Projectiles-A Plastic Wave Theory', *Int. J. Impact Engng.*, Vol. 1, pp. 393-412 (1983).
12. Taylor, G.I., 'The Use of Flat Ended projectiles for Determining Dynamic Yield Stress', *Proc. R. Soc., London, England*, A194, pp.299-299 (1948).
13. Kimsey, K., and Zukas, J.A., 'Contact Surface Erosion for Hypervelocity Problems', BRL-MR-3495, U. S. A. Ballistic Research Laboratory, Aberdeen Proving Ground, Maryland (1986).
14. Christman, D.R., and Gehring, G.W., 'Analysis of High-Velocity Projectile Penetration Mechanics', *J. Appl. Phys.*, Vol. 37, No. 4, pp. 1579-1587 (1966).

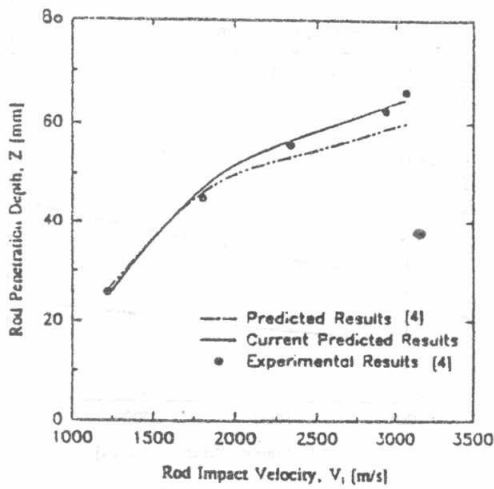


Fig. 2a. The predicted change of depth of penetration with rod impact velocity due to the high-speed impact of a tungsten rod into a tungsten target. Experimental and predicted results from Hohler and Stilp [4].

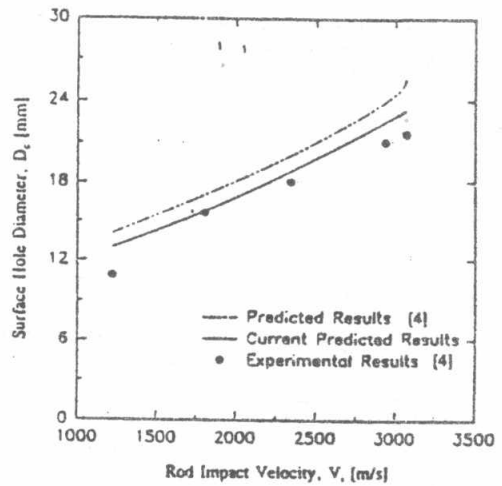


Fig. 2b. The predicted change of hole diameter with rod impact velocity due to the impact of a high-speed tungsten rod into a tungsten target. Experimental and predicted results from Hohler and Stilp [4].

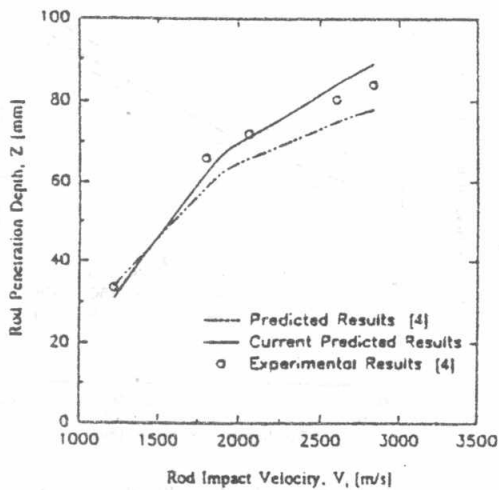


Fig. 3a. The predicted change of depth of penetration with rod impact velocity due to the high-speed impact of a tungsten rod into a steel target. Experimental and predicted results from Hohler and Stilp [4].

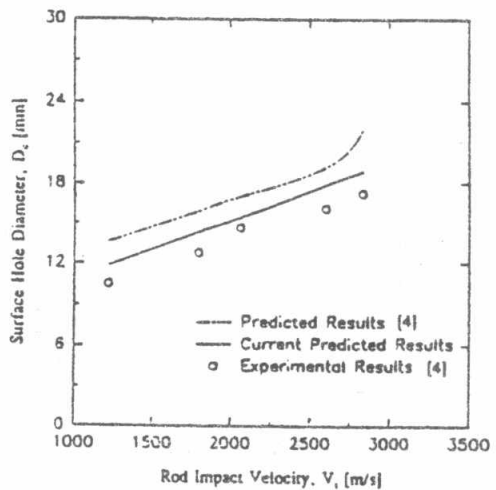


Fig. 3b. The predicted change of hole diameter with rod impact velocity due to the impact of high-speed tungsten rods into steel targets. Experimental and predicted results from Hohler and Stilp [4].

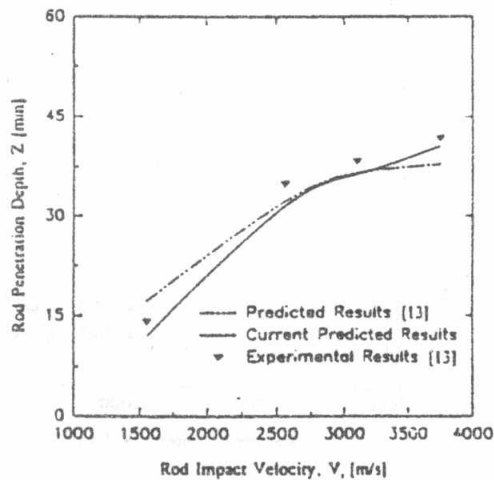


Fig. 4a. The predicted change of depth of penetration with rod impact velocity due to the high-speed impact of steel rods into steel targets. Experimental and predicted results from Kimsey and Zukas [13].

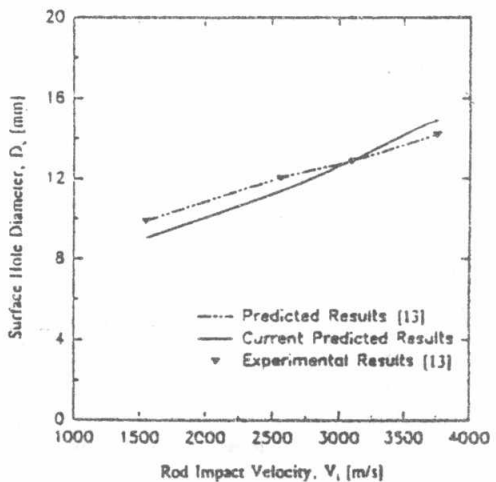


Fig. 4b. The predicted change of hole diameter with rod impact velocity due to the impact of a high-speed steel rod into a steel target. Experimental and predicted results from Kimsey and Zukas [13].

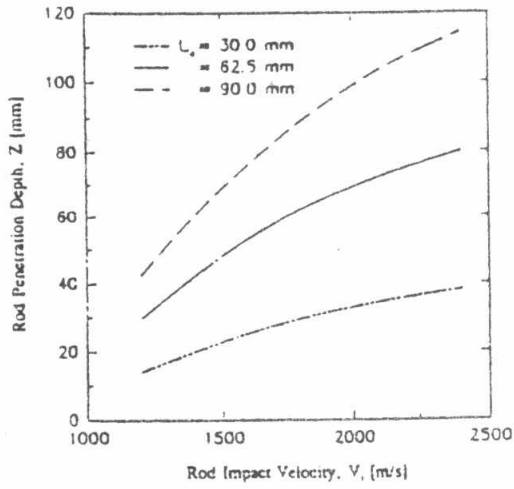


Fig. 5. The predicted change of depth of penetration with rod impact velocity for the different rod lengths.

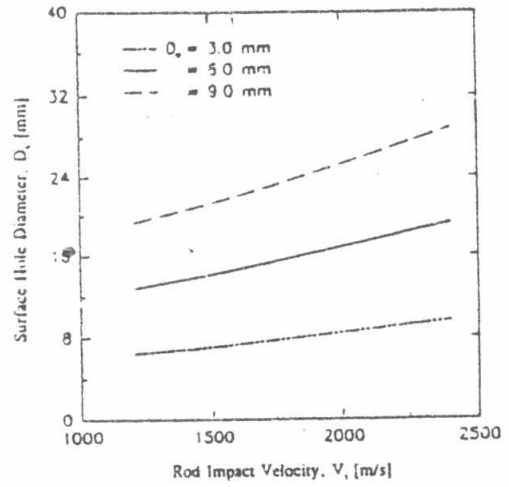


Fig. 6. The predicted change of depth of penetration with rod impact velocity for the different rod diameters.

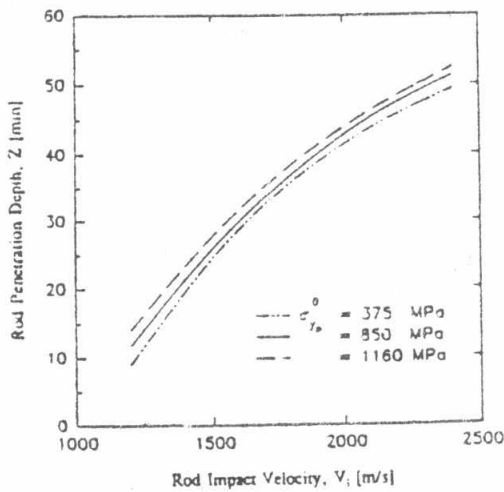


Fig. 7a. The predicted change of depth of penetration with rod impact velocity for the different rod dynamic yield strengths.

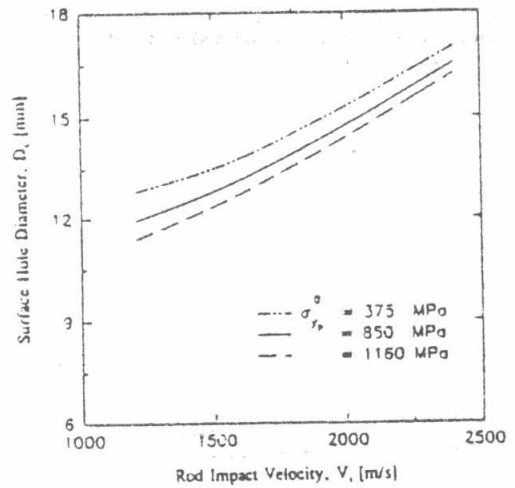


Fig. 7b. The predicted change of hole diameter with rod impact velocity for the different rod dynamic yield strengths.

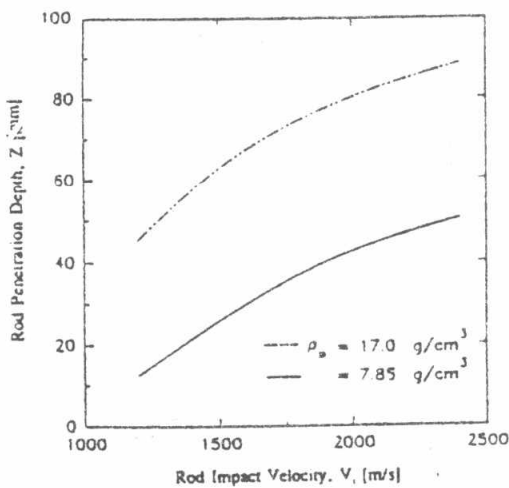


Fig. 8a. The predicted change of depth of penetration with rod impact velocity for the different rod densities.

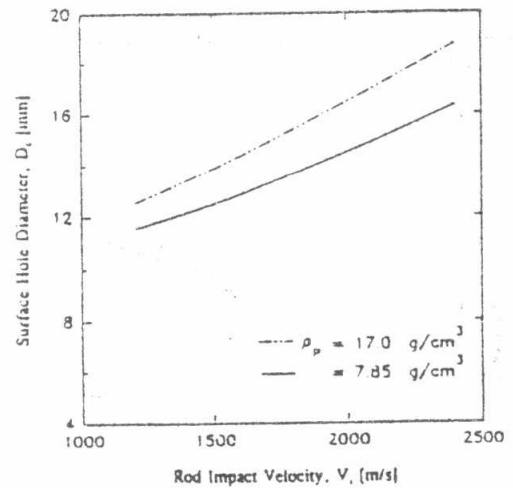


Fig. 8b. The predicted change of the hole diameter with rod impact velocity for the different rod densities.

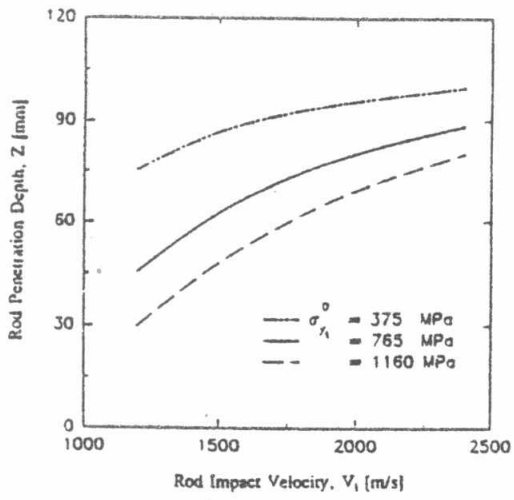


Fig. 9a. The predicted change of depth of penetration with rod impact velocity for the different target dynamic yield strengths.

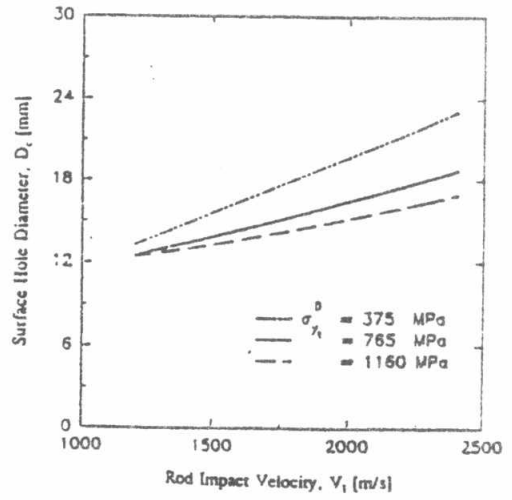


Fig. 9b. The predicted change of the hole diameter with rod impact velocity for the different target yield strengths.

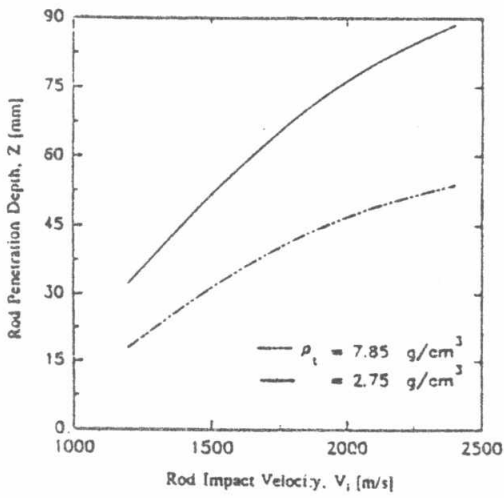


Fig. 10a. The predicted change of depth of penetration with rod impact velocity for the different target densities.

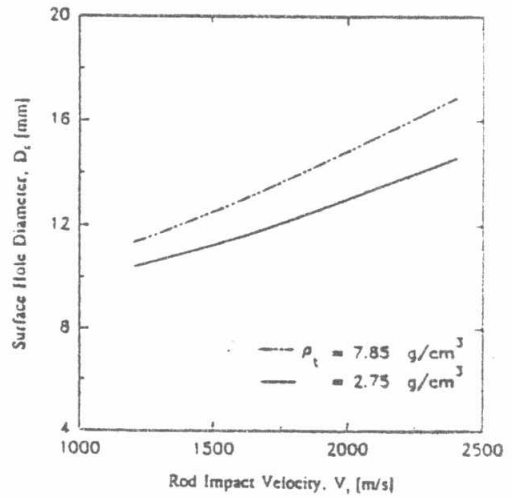


Fig. 10b. The predicted change of the hole diameter with rod impact velocity for the different target densities.